Article

Neuron

Lengthening of the Stargazin Cytoplasmic Tail Increases Synaptic Transmission by Promoting Interaction to Deeper Domains of PSD-95

Highlights

- The apparent length of the stargazin C-tail is controlled by phosphorylation
- The stargazin C-tail extension facilitates binding to PSD-95 by engaging PDZ3
- Lengthening the stargazin C-tail suffices to recruit AMPARs via lateral diffusion
- Lengthening the stargazin C-tail suffices to potentiate synaptic transmission

Authors

Anne-Sophie Hafner, Andrew C. Penn, ..., Patricio Opazo, Daniel Choquet

Correspondence

popazo@neuro.mpg.de (P.O.), dchoquet@u-bordeaux.fr (D.C.)

In Brief

Hafner et al. use nanoscale imaging to show that stargazin c-tail length determines its ability to bind PSD-95 PDZ domains deep into the cytoplasm. Stargazin c-tail extension is favored by CaMKII-induced phosphorylation, increasing activity-dependent synaptic stabilization of AMPA receptors.

Hafner et al., 2015, Neuron *86*, 475–489
April 22, 2015
http://dx.doi.org/10.1016/j.neuron.2015.03.013

CellPress

Neuron
Article

Lengthening of the Stargazin Cytoplasmic Tail Increases Synaptic Transmission by Promoting Interaction to Deeper Domains of PSD-95

Anne-Sophie Hafner,[1,2] Andrew C. Penn,[1,2] Dolors Grillo-Bosch,[1,2] Natacha Retailleau,[1,2] Christel Poujol,[3] Amandine Philippat,[1,2] Françoise Coussen,[1,2] Matthieu Sainlos,[1,2] Patricio Opazo,[1,2,4,5,*] and Daniel Choquet[1,2,3,5,*]
[1]University of Bordeaux, Interdisciplinary Institute for Neuroscience, UMR 5297, 33000 Bordeaux, France
[2]CNRS, Interdisciplinary Institute for Neuroscience, UMR 5297, 33000 Bordeaux, France
[3]Bordeaux Imaging Center, UMS 3420 CNRS, US4 INSERM, University of Bordeaux, 33000 Bordeaux, France
[4]Present address: Max Planck Institute of Neurobiology, Am Klopferspitz 18, 82152 Munich, Germany
[5]Co-senior author
*Correspondence: popazo@neuro.mpg.de (P.O.), dchoquet@u-bordeaux.fr (D.C.)
http://dx.doi.org/10.1016/j.neuron.2015.03.013

SUMMARY

PSD-95 is a prominent organizer of the postsynaptic density (PSD) that can present a filamentous orientation perpendicular to the plasma membrane. Interactions between PSD-95 and transmembrane proteins might be particularly sensitive to this orientation, as "long" cytoplasmic tails might be required to reach deeper PSD-95 domains. Extension/retraction of transmembrane protein C-tails offer a new way of regulating binding to PSD-95. Using stargazin as a model, we found that enhancing the apparent length of stargazin C-tail through phosphorylation or by an artificial linker was sufficient to potentiate binding to PSD-95, AMPAR anchoring, and synaptic transmission. A linear extension of stargazin C-tail facilitates binding to PSD-95 by preferentially engaging interaction with the farthest located PDZ domains regarding to the plasma membrane, which present a greater affinity for the stargazin PDZ-domain-binding motif. Our study reveals that the concerted orientation of the stargazin C-tail and PSD-95 is a major determinant of synaptic strength.

INTRODUCTION

PSD-95 is a major organizer and the most abundant scaffolding protein of excitatory postsynaptic densities (PSDs) (Cheng et al., 2006) in which it plays a prominent role for synaptic plasticity (Kim and Sheng, 2004). PSD-95 is a member of the membrane-associated guanylate kinase (MAGUK) family, which shares three conserved class 1 PDZ domains and one SH3-GK (Src homology 3-guanylate kinase) module (Sheng and Sala, 2001; Songyang et al., 1997). PSD-95 binds and recruits many key transmembrane proteins to the PSD, such as NMDA receptors (NMDARs); AMPA receptors (AMPARs) via binding to stargazin and other transmembrane AMPAR regulating proteins (TARPs); adhesion molecules such as Neuroligin1; several potassium channels (Kv1 and Kir 1-4); and critical neuromodulator receptors such as the β1-adrenergic receptors, the neuronal nicotinic acetylcholine receptors (nAChRc), and serotonin receptors (5-HT2A/2C Rc) (Feng and Zhang, 2009; Kim and Sheng, 2004).

Schemes have often depicted PSD-95 molecules as parallel to the postsynaptic membrane at the PSD (Kim and Sheng, 2004). Electron microscopy (EM) images of individual recombinant PSD-95 molecules (Fomina et al., 2011; Nakagawa et al., 2004) indeed show a C-shaped circular conformation consistent with results from modeling (Korkin et al., 2006). However, results from immuno-labeling EM and tomography in intact hippocampal neurons have indicated that PSD-95 is in an extended configuration and positioned into regular arrays of vertical filaments that contact both glutamate receptors and orthogonal horizontal elements layered deep inside the PSD in rat hippocampal spine synapses (Chen et al., 2008, 2011; Feng and Zhang, 2009). This is fully consistent with the fact that PSD-95 is anchored in the membrane through two palmitoylation sites located at its extreme N terminus (Craven et al., 1999; El-Husseini et al., 2000). How this perpendicular conformation might affect binding to its different partners and how this, in turn, might impact synaptic function remain unknown.

An immediate implication of an orientation of PSD-95 perpendicular to the plasma membrane is that the C-tail of transmembrane partners might need to reach out into the cytoplasm in order to bind their target domains in PSD-95. The C-tail might need to extend at least 11 nanometers—i.e., the equivalent of 30 extended amino acids—from the plasma membrane, as this distance marks the location of the first PDZ domain on PSD-95 with respect to the palmitoylation site at its extreme N terminus, as seen by EM (Chen et al., 2011). Besides these constrains, a PSD-95 perpendicular to the membrane might offer novel ways of regulating binding between PSD-95 and transmembrane proteins by modulation of the effective length of the respective intracellular domains. We explored this hypothesis using a well-characterized model: the interaction between PSD-95 and the transmembrane AMPAR auxiliary protein stargazin.

Stargazin, also called γ-2, is the first identified member of a family of TARPs found to interact directly with AMPARs and regulate their function and trafficking properties (Chen et al., 2000; Elias and Nicoll, 2007). Stargazin has a PDZ-domain-binding motif at its carboxy-terminus (C terminus) that associates directly with PSD-95-like MAGUKs, allowing it to regulate AMPAR synaptic stabilization (Bats et al., 2007; Opazo et al., 2010; Schnell et al., 2002; Tomita et al., 2005a, 2005b). Because of the critical role of the stargazin-PSD-95 interaction on AMPAR anchoring at synapses, changes in synaptic strength can be used as a functional readout (Bats et al., 2007; Chen et al., 2000; Schnell et al., 2002). Functional studies in neurons initially indicated that the AMPAR-stargazin complex preferentially binds to either or both of the PSD-95 first two PDZ domains (Schnell et al., 2002; Xu et al., 2008). These first two PDZ domains stand out as a functional supramodular ensemble in which the relative orientation of the two ligand-binding grooves favors accommodating multiple ligands originating from the same direction, as seen by nuclear magnetic resonance (NMR) (Long et al., 2003; Wang et al., 2009), X-ray crystallography (Sainlos et al., 2011), and Förster resonance energy transfer (FRET) with the full-length protein (McCann et al., 2011). It is interesting to note that, in an extended PSD-95 conformation, PDZ1 and 2 are the closest to the membrane and, therefore, might preferentially contribute to binding due to their proximity to the PDZ-binding motif of stargazin. Finally, the anchoring of TARP-containing AMPARs at the synapse likely involves multivalent PDZ-domain-mediated interactions (Fomina et al., 2011; Pegan et al., 2007). This idea is consistent with the development of synthetic divalent ligands that were designed to replicate the multiplicity of stargazin C termini per AMPAR complex. These biomimetic divalent ligands could specifically and acutely disrupt the endogenous AMPAR-MAGUK interaction in cultured neurons in conditions where a single competing binding motif had no effect (Sainlos et al., 2011).

About 100 amino acids upstream of the C-terminal PDZ-binding motif, the stargazin C-tail harbors a stretch of seven arginines interleaved by nine serines (RS domain) (Figure S1A), so that the overall charge of this domain is highly positive. Previous studies have shown that the RS domain is attached to the plasma membrane via electrostatic interactions with negatively charged phospholipids (Roberts et al., 2011; Sumioka et al., 2010). This membrane interaction may reduce what we called the ''effective'' length of the C-tail and thus further constrain binding by limiting the ability of stargazin PDZ-binding motif to sample efficiently the spine cytoplasm. Notably, it has been shown that the serine residues present in the RS domain can be phosphorylated in an activity-dependent manner by CaMKII and PKC (Tomita et al., 2005b) so that the RS domain changes from highly positive to negative upon phosphorylation. More important, phosphorylation seems to disrupt the electrostatic interaction between the membrane and the stargazin C-tail (Sumioka et al., 2010). Additionally, biochemical and functional studies have demonstrated that phosphorylation of the RS domain facilitates the interaction between stargazin and PSD-95 (Opazo et al., 2010; Sumioka et al., 2010; Tomita et al., 2005b). Taken together, these findings raise the intriguing possibility that phosphorylation might regulate binding to PSD-95 simply by increasing the effective length of the stargazin C-tail, thus facilitating access to PDZ domains deeper in the spine cytoplasm.

In this study, we took advantage of super-resolution imaging techniques, biophysical measurements, biochemistry, and electrophysiology to show that the effective length of the stargazin C-tail, rather than the one defined by the primary sequence, is the major factor controlling not only binding to PSD-95 but also the recruitment of AMPARs and, thus, the strength of synaptic transmission.

RESULTS

In the first set of experiments, we developed a tool with nanoscale precision to specifically monitor changes in the relative distance between the stargazin PDZ-domain-binding motif and the plasma membrane. We designed a specific FRET pair between the plasma membrane marker R18 (octadecyl rhodamine B chloride) and stargazin::GFP (Figure 1A). We expressed stargazin::GFP_{267} (where GFP was positioned immediately after the putative membrane-bound RS region of the stargazin C-tail; Figure S1A) in cultured hippocampal neurons and stained neurons with R18 prior to imaging (Figure 1B). We then used fluorescence lifetime imaging microscopy (FLIM) to estimate the degree of FRET by measuring the decrease in GFP lifetime (Yasuda, 2006). We found a robust FRET signal between stargazin::GFP_{267} and R18 (Figure 1C). Notably, there was no FRET between soluble GFP and R18, arguing for a specific FRET signal in the vicinity of the plasma membrane. In order to examine whether the rest of the C-tail extended into the cytoplasm, we positioned GFP further down the C-tail (stargazin::GFP_{302}) and measured its interaction with R18. As expected for a tail oriented perpendicular to the membrane, this construct displayed a weaker FRET signal, indicating that this region is statistically further away from the plasma membrane. We then positioned GFP even further down the C-tail (stargazin::GFP_{322}) and found an even weaker FRET with R18, consistent with the idea that the C-tail is extending away from the plasma membrane, into the cytoplasm (Figure 1C). Thus, as opposed to the membrane attachment of the proximal region of the stargazin C-tail, the distal half carrying the PDZ-binding motif displays an extended conformation as might be needed if they are to reach the PDZ domains of an extended PSD-95.

Recent biochemical and functional studies have demonstrated that the interaction between stargazin and PSD-95 can be regulated by phosphorylation of the serine stretch in the stargazin C-tail (Opazo et al., 2010; Sumioka et al., 2010; Tomita et al., 2005b). Notably, phosphorylation seems to disrupt the electrostatic interaction between the membrane and the stargazin C-tail. This finding raises the intriguing possibility that phosphorylation might further extend the distal half of the stargazin C-tail into the cytoplasm, thus increasing its effective length in order to facilitate access to PDZ domains deeper in the cytoplasm of spines. In order to examine this hypothesis, we introduced phospho-mutations to the stargazin::GFP_{267} construct used earlier (Figure 1D). We mimicked stargazin phosphorylation by mutating the nine phosphorylated serine residues to aspartates (stargazin::GFP_{267} S9D) and measured the interaction of this construct with the plasma membrane. We found that these

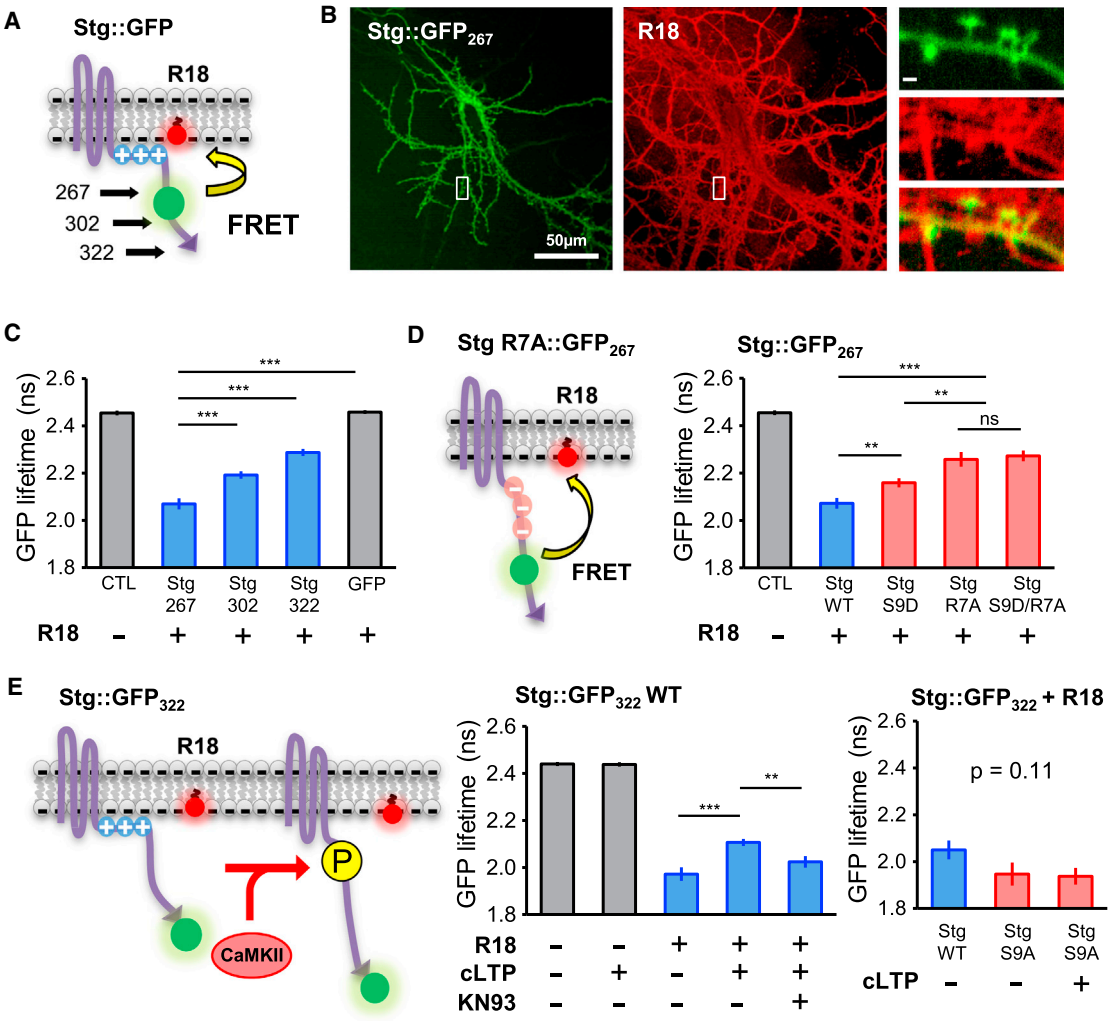

Figure 1. The Stargazin C-tail Effectively Extends into the Cytoplasm in a Charge-Dependent Manner

The interaction between the Stg C terminus and the plasma membrane was studied using a two-photon-based FRET-FLIM technique.

(A) Scheme (left) showing that GFP inserted into the Stg C terminus at various positions is in close proximity to the membrane labeled with R18 and can be detected by FRET.

(B) Images of a neuron expressing Stg::GFP (left) and incubated for 5 min at 37°C with R18 (middle). Scale bar, 50 µm. Zoom onto a dendrite portion (right). Stg::GFP is expressed in the dendritic shaft and enriched in spine heads (top panel at right). R18 labels the plasma membrane uniformly (middle panel at right). Overlay of the Stg::GFP and R18 images showing that neurons transfected with Stg::GFP are efficiently labeled with R18 (bottom panel at right). Scale bar for top panel at right, 1 µm.

(C) GFP lifetime is decreased in the presence of R18 (10 µM) when the GFP is coupled to Stg (CTL = 2.441 ns, n = 20; Stg::GFP$_{267}$ = 2.076 ns, n = 34; Stg::GFP$_{302}$ = 2.167 ns, n = 16; Stg::GFP$_{322}$ = 2.288, ns, n = 22) but not when GFP is freely diffusing in the cytoplasm (GFP = 2.459 ns, n = 16). $p < 0.0001$, Welch's ANOVA. CTL, control.

(D) Scheme (left) showing the expected elongation of Stg C terminus when the RS domain is negatively charged. Mutations affecting the charge of the RS domain modify the efficacy of the energy transfer from the GFP to R18 (10 µM) (right) (CTL = 2.455 ns, n = 18; WT = 2.072 ns, n = 44; S9D = 2.159 ns, n = 40; R7A = 2.272 ns, n = 20; S9D/R7A = 2.258 ns, n = 22). $p < 0.0001$, Welch's ANOVA.

(E) Scheme (left) showing the expected re-localization of Stg PDZ-binding motif after CaMKII phosphorylation. Following cLTP induction, the efficiency of energy transfer from GFP to R18 (20 µM) is reduced (right) (basal −R18 = 2.440 ns, n = 14; cLTP −R18 = 2.438 ns, n = 11; Basal +R18 = 1.972 ns, n = 26; cLTP +R18 = 2.107 ns, n = 43). This effect is blocked by CaMKII inhibitor KN93 (cLTP +KN93 +R18 = 2.024 ns, n = 28) and Stg S9A mutation (WT −cLTP = 2.050 ns, n = 19; S9A −cLTP = 1.947 ns, n = 18; S9A +cLTP = 1.938 ns, n = 22). $p < 0.0001$, Welch's ANOVA.

Data represented as mean ± SEM. $^{**}p < 0.01$; $^{***}p < 0.0005$; ns, not significant (p = 0.11).

phospho-mimetic mutations extend the stargazin C-tail into the cytoplasm of spines as reflected by a decrease in FRET with R18 in the membrane (Figure 1D). We also confirmed that phospho-mutations also extended the C-tail of stargazin carrying the GFP further down the C-tail and thus better reflecting the behavior of the PDZ-domain-binding motif (stargazin::GFP$_{302}$ S9D/R7A) (Figure S1B). To control that the increase in GFP lifetime was due to the distancing of the stargazin C-tail from the

plasma membrane and not due to a nonspecific effect on the intrinsic properties of GFP (i.e., alterations in the dipole orientation), we designed a second FRET pair between stargazin::mCherry$_{302}$ and the plasma membrane marker F18 (fluorescein octadecyl ester) as a FRET donor. Similarly, we found that the introduction of phospho-mimetic mutations distanced the cytoplasm tail of stargazin::mCherry away from the plasma membrane, as evidenced by the increase in F18 lifetime (Figures S1C and S1D).

Together, these findings strongly suggest that phosphorylation further extends the distal half of the stargazin C-tail carrying the PDZ-domain-binding motif in order to facilitate access and binding to PDZ domains that would be located further away from the membrane, such as in a PSD-95 oriented perpendicularly to the plasma membrane.

Since the proximal half of the stargazin C-tail is presumably bound to the membrane via a stretch of positively charged arginine residues, we examined whether mutating these residues was sufficient to extend the distal half into the cytoplasm. We found that substituting the seven arginine residues to uncharged alanines (stargazin::GFP$_{267}$ R7A) was sufficient to extend the distal half of the C-tail into the cytoplasm (Figure 1D). In addition, the combined mutant stargazin::GFP$_{267}$ S9D/R7A did not exhibit additive effects, suggesting that phosphorylation extends the stargazin C-tail into the cytoplasm solely by neutralizing the positively charged arginine residues.

Next, we examined whether the stargazin C-tail can be extended after induction of CaMKII activity. Using the FRET pair between stargazin::GFP$_{322}$ wild-type (WT) and R18 in cultured hippocampal neurons, we activated NMDARs via a chemically induced long-term potentiation (cLTP) protocol known to promote the CaMKII-dependent immobilization of AMPAR (Opazo et al., 2010). We found that the cLTP protocol was sufficient to extend the stargazin C-tail away from the plasma membrane (Figure 1E). It is important to note that the cLTP-induced extension of the stargazin C-tail was mediated by direct phosphorylation of stargazin by CaMKII, as it was significantly reversed by the CaMKII inhibitor KN93 and was not observed when the stretch of nine serines in stargazin was substituted by non-phosphorylatable alanines (S9A).

Although phosphorylation increases the extension of the stargazin C-tail away from the membrane, it remains unclear whether this phenomenon alone can account for the facilitated binding to PSD-95 that was previously observed in Sumioka et al. (2010). It is also possible that phosphorylation might create binding sites to additional proteins that might ultimately stabilize the stargazin-PSD-95 complex. In order to discriminate between these possibilities, we first wanted to confirm that stargazin phosphorylation does, in fact, facilitate binding to PSD-95 as it has been previously reported (Sumioka et al., 2010). To that end, we co-expressed untagged PSD-95 with stargazin WT, stargazin S9D, or stargazin S9A in COS-7 cells and examined their relative interaction using pull-down assays. As previously observed, we found that PSD-95 preferentially pulled down the phospho-mimetic stargazin S9D. In addition, PSD-95 displayed a stronger interaction with stargazin WT than with the stargazin S9A (Figure 2A). As a control for our FRET experiments, we verified that PSD-95::GFP displayed the same behavior in pull-down assays as untagged PSD-95 (Figure S2A).

To examine whether stargazin phosphorylation bi-directionally regulates binding to PSD-95 in living cells, we co-transfected stargazin::mCherry and PSD-95::GFP in COS-7 cells (Figure 2B), introduced phospho-mutations to the stargazin::mCherry C-tail (stargazin::mCherry S9A and S9D) (Tomita et al., 2005b), and measured the degree of FRET through GFP lifetime (Sainlos et al., 2011). Stargazin::mCherry S9D facilitated the interaction with PSD-95::GFP as reflected by the decrease in GFP lifetime (Figure 2B). Intriguingly, we found no difference between stargazin::mCherry WT and stargazin::mCherry S9A on binding PSD-95::GFP using our FRET assay (Figure 2B). It is possible that stargazin::mCherry WT might not be normally phosphorylated in COS-7 cells (and, therefore, behave similarly to stargazin S9A), either because of a lack of CaMKII activity or because the bulky size of the acceptor fluorophore mCherry might prevent CaMKII access. We believe the latter scenario is the most likely for two reasons. First, the pull-down assays described earlier using stargazin not tagged with fluorescent proteins showed a differential binding between stargazin WT and S9A, suggesting endogenous phosphorylation of stargazin WT RS domain in COS-7 cells. Second, we found that active CaMKII failed to facilitate binding between stargazin::mCherry WT and PSD-95::GFP using FRET (data not shown). However, CaMKII did facilitate the stargazin-PSD-95 interaction when stargazin WT was labeled with the small acceptor fluorophore ReAsH (molecular weight [MW], 0.58 kDa), using the TetraCysteine system instead of a bulkier fluorescent protein (Figure 2C). This CaMKII-induced increase in stargazin-PSD-95 interaction was absent when the nine serines on the stargazin C-tail, which are the CaMKII substrates, were mutated to alanines (S9A).

Finally, we tested whether the stargazin phosphorylation state might also regulate binding to PSD-95 in neurons. To that end, we measured the extent of FRET between PSD-95::GFP and either stargazin WT or S9D in cultured hippocampal neuron. As shown in Figures 2D–2F, we found that PSD-95::GFP presents a stronger interaction with stargazin::mCherry S9D at both spines and dendritic shaft, as evidenced by the robust decrease in GFP lifetime. Notably, stargazin WT only interacted with PSD-95 in spines but not in dendritic shafts. The S9D and R7A mutations induced the interaction of stargazin with PSD-95 in dendritic shafts and potentiated that in spines (Figure 2F). As observed previously in COS-7 (Figure 2B), stargazin WT and S9A displayed a similar interaction with PSD-95. Again, this indicates that stargazin::mCherry WT is most likely not phosphorylated.

As a control, we verified that PSD-95::GFP co-localized with both stargazin::mCherry WT and S9D (Figure S2B) and that expression of the latter did not modify PSD-95 distribution between synaptic and extra-synaptic compartments (Figure S2C). In addition, taking advantage of the capacity of our FRET-FLIM instrument to perform spatial maps, we found no significant proximal-to-distal dendrite spatial gradient in FRET signal between PSD-95::GFP and stargazin::mCherry WT or S9D (Figure S2D).

Having confirmed that stargazin phosphorylation facilitates binding to PSD-95 in living COS-7 cells and cultured neurons,

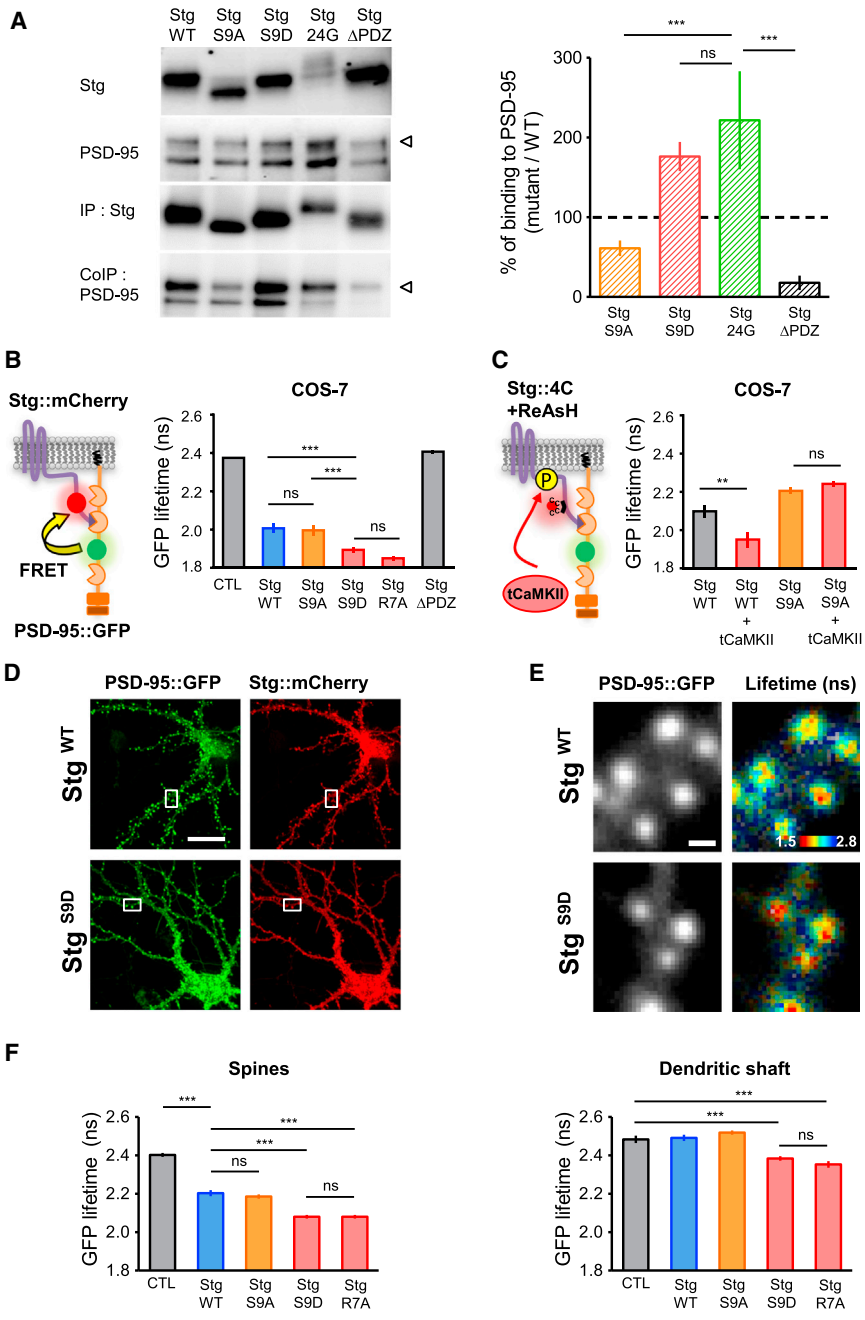

Figure 2. The Stargazin C-tail Charge Regulates Binding to PSD-95 in Neurons

(A) COS-7 cells expressing PSD-95 WT and HA-Stg. PSD-95 preferentially co-immunoprecipitates with Stg mutants with extended C-terminal domains (CTDs) (S9D and 24G). Before immunoprecipitation (IP), cells were incubated with dithiobis(succinimidylpropionate) (DSP). Representative western blots for total protein (top: Stg, second row: PSD-95), immunoprecipitation (IP), or co-immunoprecipitation (CoIP) of PSD-95 for the different Stg mutants. The same gel of starting material is blotted for PSD-95 and stargazin. The arrows show the upper band of PSD-95 that was used for quantifications (left). Quantified blot data for each condition (right) (S9A = 61%; S9D = 176%; 24G = 222%; ΔPDZ = 18%) measuring the ratio of PSD-95 co-immunoprecipitated over the immunoprecipitated stargazin. Data are normalized to the control condition Stg WT. Columns are compared using ANOVA and Tukey post-test. The bar graph shows the mean and 95% confidence intervals.

(B) Scheme representing the FRET pair PSD-95 coupled to the donor GFP inserted between PDZ domains 2 and 3 (PSD-95::GFP$_{253}$) and Stg coupled to the acceptor mCherry (left). In COS-7 expressing this FRET pair, Stg phospho-mimetic mutation increases binding to PSD-95::GFP (right) (CTL = 2.375 ns, n = 21; Stg WT = 2.007 ns, n = 35; Stg S9A = 1.996 ns, n = 40; Stg S9D = 1.894 ns, n = 157; Stg R7A = 1.850 ns, n = 70; Stg ΔPDZ = 2.407 ns, n = 16). ANOVA and Bonferroni post-test. CTL, control.

(C) Scheme representing the FRET pair PSD-95::GFP$_{253}$ and Stg coupled to a TetraCysteine tag (Stg::4C) binding specifically to the membrane-permeable acceptor fluorophore ReAsH (left). Constitutively active truncated CaMKII (tCaMKII) increases binding between PSD-95 and Stg in COS-7 cells (right) (Stg WT = 2.098 ns, n = 51; Stg WT +tCaMKII = 1.951 ns, n = 55). The tCaMKII effect is blocked by Stg S9A mutation (Stg S9A = 2.205 ns, n = 48; Stg S9A +tCaMKII = 2.242 ns, n = 45). Data were compared using Student's t test.

(D) Images of cultured hippocampal neurons (12 days in vitro; DIV) expressing PSD-95::GFP$_{400}$ (left) and Stg::mCherry (right). Scale bar, 20 μm.

(E) Zooms on a dendrite portion with spines representing the PSD-95::GFP$_{400}$ channel (left) and the color-coded GFP lifetime intensity (right). Scale bar, 1 μm.

(F) Stg phosphomimetic mutant S9D and R7A mutant increase binding to PSD-95 in spines (left) (CTL = 2.402 ns, n = 128 spines, 13 cells; WT = 2.203 ns, n = 96 spines, 10 cells; S9A = 2.185 ns, n = 175 spines, 15 cells; S9D = 2.080 ns, n = 240 spines, 24 cells; Stg R7A = 2.080 ns, n = 160 spines, 16 cells) and induce binding to PSD-95 in dendritic shaft (right) (CTL = 2.483 ns, n = 65 dendritic shaft areas, 13 cells; WT = 2.491 ns, n = 119 dendritic shaft areas, 10 cells; S9A = 2.519 ns, n = 84 dendritic shaft areas, 15 cells; S9D = 2.384 ns, n = 205 dendritic shaft areas, 24 cells; R7A = 2.353 ns, n = 60 dendritic shaft areas, 10 cells). $p < 0.0001$, Welch's ANOVA.

Data are represented as mean ± SEM. $^{**}p < 0.01$; $^{***}p < 0.0005$; ns, not significant. Post-test results are from pairwise Welch's two-tailed t tests with Shaffer's step-wise Bonferroni procedure.

we investigated whether this facilitation results directly from the extension of the stargazin C-tail toward the cytoplasm. As a first approximation to this question, we reasoned that, if the charge of the stargazin C-tail is the critical factor controlling binding to PSD-95, then mutating the arginine residues to modify this charge should be sufficient to facilitate binding to PSD-95. Indeed, mutating the seven arginines to alanines (stargazin::mCherry$_{302}$ R7A) was sufficient to facilitate binding to PSD-95 (Figure 2F). Since stargazin R7A is also sufficient to extend the stargazin C-tail into the cytoplasm (Figure 1D), it is

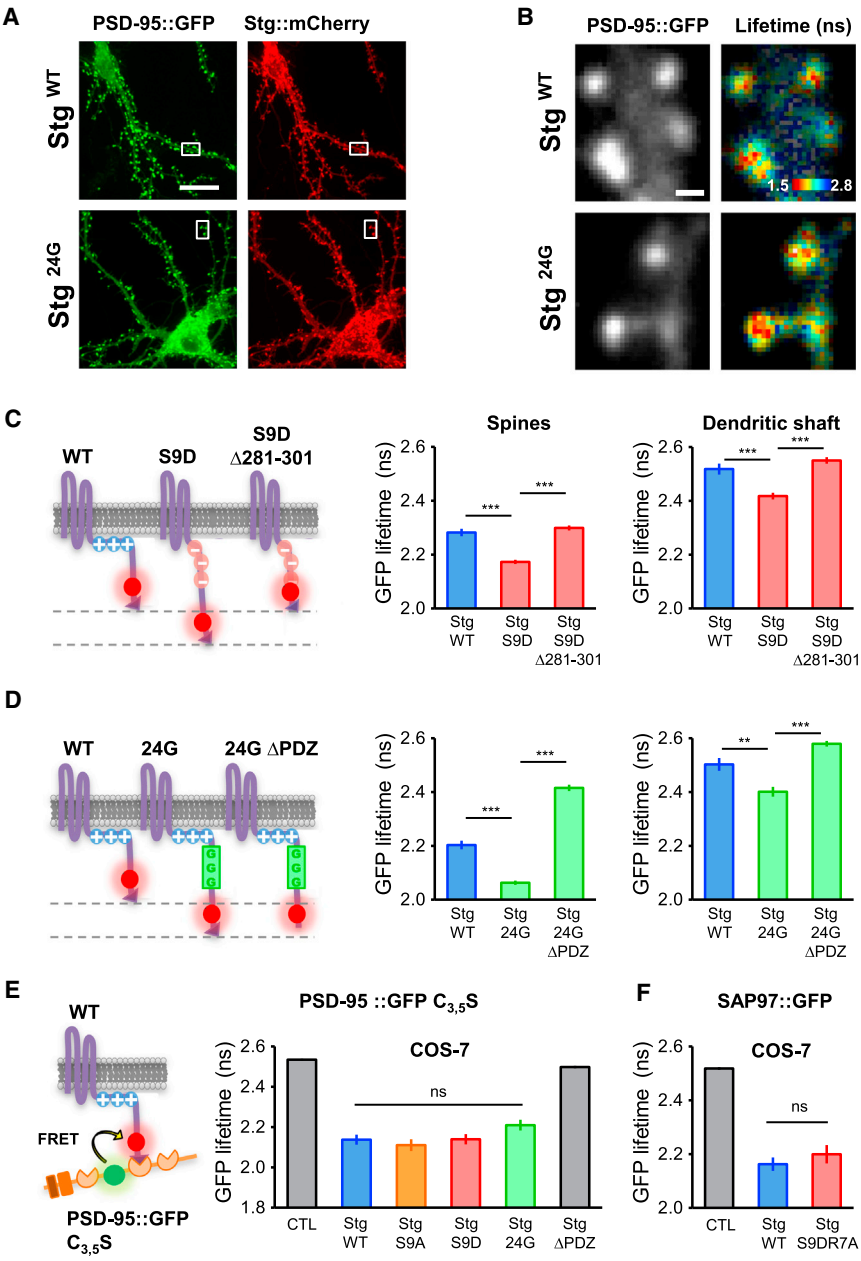

Figure 3. The Effective Extension of the Stargazin C-tail Is Necessary and Sufficient to Facilitate Binding to PSD-95 in Neurons

(A) Images of hippocampal culture neurons (12 DIV) expressing PSD-95::GFP_{400} (left) and Stg::mCherry (right). Scale bar, 20 μm.

(B) Zooms on portion of dendrites with spines representing the GFP channel (left) and color-coded GFP lifetime intensity (right). Scale bar, 1 μm.

(C) Neurons expressing the FRET pair PSD-95::GFP_{253} and Stg::mCherry. Schemes of the constructs used showing that we generated a Stg S9D mutant with a shorter CTD by truncating 20 amino acids between the RS domain and the mCherry (left). The truncation is sufficient to block the S9D effect in spines (middle) (WT = 2.282 ns, n = 83 spines, 9 cells; S9D = 2.173 ns, n = 279 spines, 28 cells; S9DΔ281–301 = 2.299 ns, n = 251 spines, 26 cells) and dendrites (right) (WT = 2.518 ns, n = 30 regions, 9 cells; S9D = 2.418 ns, n = 96 regions, 28 cells; S9DΔ281–301 = 2.550 ns, n = 90 regions, 26 cells). $p < 0.0001$, Welch's ANOVA.

(D) Hippocampal cultured neurons expressing the FRET pair PSD-95::GFP_{400} and Stg::mCherry. Schemes of the constructs used showing that we generated a Stg WT with an extended CTD by inserting a glycine linker of 24 amino acids after the RS domain (left). Stretching out the Stg CTD is sufficient to mimic the S9D effect in spines (middle) (WT = 2.203 ns, n = 96 spines, 10 cells; 24G = 2.049 ns, n = 176 spines, 18 cells; 24GΔPDZ = 2.418 ns, n = 74 spines, 6 cells) and dendrites (right) (WT = 2.503 ns, n = 36 regions, 10 cells; 24G = 2.401 ns, n = 66 regions, 18 cells; 24GΔPDZ = 2.580 ns, n = 36 regions, 6 cells). $p < 0.0001$, Welch's ANOVA.

(E) Scheme representing the FRET pair PSD-95::GFP_{253} C3,5S mutated for its two N-terminal palmitoylation sites and Stg::mCherry (left). In COS-7 expressing this FRET pair, Stg with elongated CTD do not show increase binding to PSD-95 (right) (CTL = 2.535 ns, n = 37; WT = 2.138 ns, n = 41; S9A = 2.110 ns, n = 40; S9D = 2.139 ns, n = 40; 24G = 2.210 ns, n = 39; ΔPDZ = 2.498 ns, n = 14). $p < 0.0001$, Welch's ANOVA, comparing all conditions of PSD-95::GFP C3,5S- and Stg::mCherry-expressing cells. CTL, control.

(F) COS-7 cells expressing the FRET pair SAP97::GFP and Stg::mCherry. This binding is not regulated by the Stg RS domain charge (CTL = 2,518, n = 60; STG WT = 2.163 ns, n = 88; STG S9D/R7A = 2.199 ns, n = 90).

Data are represented as mean ± SEM. **p < 0.01; ***p < 0.0005; ns, not significant. Post-test results are from pairwise Welch's two-tailed t tests with Shaffer's step-wise Bonferroni procedure.

likely that the effective length of the stargazin C-tail is the major determinant in the facilitated interaction with PSD-95.

We then performed two additional experiments to directly confirm that the effective length of the stargazin C-tail is the critical factor controlling binding to PSD-95 (Figures 3A–3D). First, we argued that, if stargazin S9D has a stronger interaction with PSD-95 because of a longer effective C-tail, then shortening the C-tail of stargazin S9D by a truncation might effectively block the facilitated binding to PSD-95. As shown in Figure 3C, a small truncation in the distal half of stargazin C-tail S9D (Stargazin::mCherry S9D Δ281–301, the PDZ-binding motif still present) was sufficient to block the facilitation of binding to PSD-95. Second, in order to examine whether an extension of the stargazin C-tail alone would be sufficient to facilitate binding to PSD-95, we introduced a linker of 24 glycine residues immediately after the membrane-bound proximal half of WT stargazin (stargazin::mCherry 24G). Strikingly, we found that the presence of the linker was sufficient to facilitate binding to PSD-95 in a

PDZ-domain-dependent manner using FRET (Figures 3A and 3D) and pull-down assays (Figure 2A). It is important to note that we used the FRET pair between stargazin::mCherry and the plasma membrane marker F18 to ensure that the insertion of the 24G linker effectively extended the stargazin C-tail into the cytoplasm (Figure S3). Taken together, these findings indicate that increasing the effective length—and, hence, extension into the cytoplasm—of the stargazin C-tail is both necessary and sufficient to facilitate access and binding to the PDZ domains of PSD-95.

Based on our working model, we reasoned that stargazin carrying elongated C-tails such as S9D or 24G should have an enhanced binding to PSD-95 only in the context of a PSD-95 oriented perpendicularly to the plasma membrane because they can reach deeper PDZ domains. Given that the N-terminal palmitoylation of PSD-95 is essential to adopt such orientation, we examined whether preventing palmitoylation might disrupt the perpendicular orientation of PSD-95 and, as a consequence, whether stargazin S9D and 24G would lose their enhanced binding abilities. To test this hypothesis, we measured by FRET in COS-7 cells the interaction between non-palmitoylatable PSD-95 $C_{3,5}S$—in which the two palmitoylation substrate cysteine residues on the PSD-95 N terminus are mutated to serines—and all the different stargazin mutants. PSD-95 $C_{3,5}S$ equally interacted with all stargazin mutants, including WT, S9A, S9D, and 24G (Figure 3E). In a related experiment, we designed a FRET pair between stargazin::mCherry and SAP97::GFP, a non-palmitoylatable member of the MAGUK family of scaffold proteins. Stargazin S9D did not facilitate binding to SAP97 (Figure 3F). Together, these results are in line with the notion that stargazin phosphorylation facilitates binding to PSD-95 simply by increasing the "apparent" length of stargazin C-tail. At the same time, they suggest that the orientation of both the stargazin C-tail and PSD-95 function in concert to facilitate binding.

As might be expected from a PSD-95 containing three PDZ domains and oriented perpendicularly to the membrane, our model predicts that stargazin with elongated C-tails could bind to PDZ domains further away from the membrane. In other words, stargazin WT might preferentially bind PDZ1 (closer to the membrane), whereas stargazin S9D might preferentially bind PDZ3 (Figure 4A). If this is true, then PSD-95 carrying mutations in PDZ1 should preferentially disrupt the interaction with stargazin WT, whereas PSD-95 carrying mutations in PDZ3 should preferentially impact binding to stargazin S9D. As predicted by this model, we found that PSD-95 with a mutated PDZ1 (PSD-95::GFP H130V) selectively reduced binding to stargazin WT but had no effect on binding to stargazin S9D (Figure 4B). On the contrary, PSD-95 with a mutated PDZ3 (PSD-95::GFP H372V) had a greater effect on stargazin S9D than on stargazin WT (Figure 4D). In addition, we found that PSD-95 carrying a mutation in PDZ2 (PSD-95::GFP H225V) has a similar impact on both stargazin WT and S9D (Figure 4C). Together, these observations are consistent with the hypothesis that an extended C-tail facilitates access to the farthest located PDZ domain, PDZ3, in a perpendicularly oriented PSD-95 toward the plasma membrane.

In order to confirm that stargazin-S9D-facilitated binding to PSD-95 is mediated by the PDZ3 domain, we designed a competition assay by triple transfecting the FRET pair PSD-95::GFP and stargazin::mCherry WT along with stargazin S9D not tagged with a fluorescent protein. Although we observed a strong FRET signal between PSD-95::GFP and stargazin::mCherry WT, we found that co-expressing non-tagged stargazin S9D outcompeted stargazin::mCherry WT, as shown by a reduction in FRET (Figure S4A). As a control, we found that non-fluorescent stargazin WT did not outcompete stargazin::mCherry WT. Using this competition assay, we examined whether stargazin S9D might preferentially bind to the PDZ3 domain of PSD-95. Even though stargazin S9D strongly disrupted the interaction between PSD-95::GFP and stargazin::mCherry WT, it was unable to disrupt the interaction between stargazin::mCherry and PSD-95::GFP carrying a PDZ3 mutation (Figures S4B and S4C). On the other hand, stargazin S9D still disrupted the interaction between stargazin::mCherry and PSD-95::GFP carrying a PDZ1 mutation.

To independently confirm the role of the PDZ3 domain in mediating the effects of stargazin S9D, we used a co-immunoprecipitation assay. Even though untagged stargazin S9D strongly facilitated binding to PSD-95, it no longer facilitated binding to PSD-95 carrying a PDZ3 mutation. On the other hand, stargazin S9D still facilitated binding to PSD-95 carrying a PDZ1 mutation (Figures S5A and S5B).

Taken together with our previous FRET findings, these sets of experiments strongly indicate that stargazin carrying "elongated" C-tails, such as S9D, preferentially bind to the "deeper" PDZ3 domains on PSD-95.

Given that stargazin with an extended C-tail (S9D or linker) enhanced the overall binding to PSD-95, we were intrigued that just shifting the binding from PDZ1 to PDZ3 would, in fact, increase net binding to PSD-95. A possible explanation for this observation would be that the PDZ-domain-binding motif of stargazin has a higher affinity for PDZ3 than for PDZ1. To test this hypothesis, we measured the binding affinity between a peptide containing the PDZ-domain-binding motif of stargazin and the individualized recombinant PDZ domains of PSD-95 using fluorescence polarization-based titrations. Indeed, the PDZ-domain-binding motif of stargazin has more than 3-fold higher affinity for PDZ3 than for PDZ1 (rPDZ1, K_D [dissociation constant] = 43.2 ± 3.0 μM; versus rPDZ3, K_D = 13.7 ± 0.6 μM) (Figure 5). In addition, the PDZ-binding motif of stargazin has the highest affinity for PDZ2 (rPDZ2, K_D = 3.4 ± 0.5 μM). Altogether, these measurements suggest that the extension of stargazin C-tail enhances the overall binding to PSD-95 by shifting to the farthest and highest affinity PDZ2/PDZ3 domains.

In the last set of experiments, we set out to define the functional impact of stargazin carrying an elongated C-tail. We and others have previously shown that the interaction between stargazin and PSD-95 is central for the synaptic immobilization and recruitment of AMPARs (Bats et al., 2007; Opazo et al., 2012; Schnell et al., 2002). In order to examine whether stargazin carrying an elongated C-tail was sufficient to immobilize AMPARs, we expressed PSD-95::GFP together with stargazin WT or carrying a 24G linker. We monitored the surface mobility of AMPARs using a single-particle tracking approach. Endogenous-surface-expressed GluA2-containing AMPARs were sparsely labeled in live neurons with anti-GluA2 antibody-coupled QDots, and their

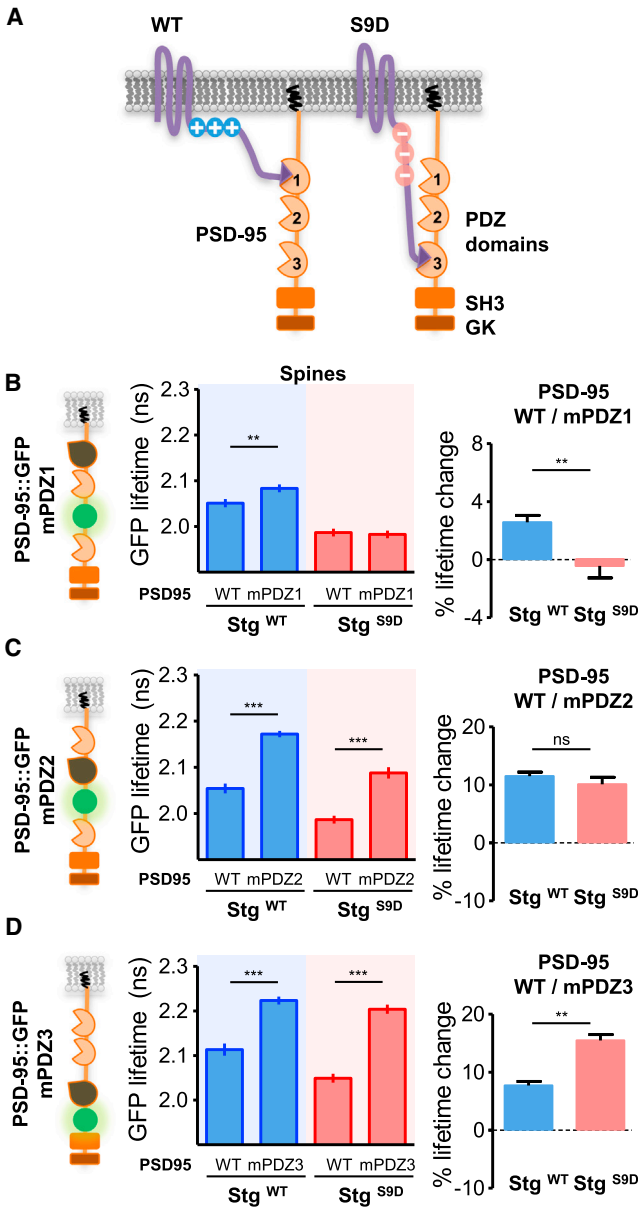

Figure 4. The Effective Extension of the Stargazin C-tail Preferentially Engages Binding to the Farthest Located PDZ3 Domain of PSD-95

(A) Schemes of our working model that Stg with elongated CTD has greater access to deeper PDZ domains of PSD-95.

(B) Hippocampal cultured neurons (12–14 DIV) transfected with the FRET pair Stg::mCherry WT or S9D and PSD-95::GFP$_{253}$ mPDZ1 with the GFP inserted between PDZ domains 2 and 3 (left). Impairment of the binding to PSD-95 first PDZ domain by expressing PSD-95 mPDZ1 (H130V single point mutation on the full-length PSD-95) reduces Stg::mCherry WT binding to PSD-95 but not Stg::mCherry S9D (middle) (Stg WT + PSD-95 WT = 2.051 ns, n = 230 spines, 23 cells; Stg WT + PSD-95 mPDZ1 = 2.083 ns, n = 283 spines, 29 cells; Stg S9D + PSD-95 WT = 1.987 ns, n = 288 spines, 30 cells; Stg S9D + PSD-95 mPDZ1 = 1.983 ns, n = 259 spines, 27 cells). The relative lifetime change shows that PDZ1 contributes only to the binding of Stg WT (right) (Stg WT = 0.026 a.u.; Stg S9D = −0.004 a.u.).

(C) Neurons transfected with the FRET pair Stg::mCherry WT or S9D and PSD-95::GFP$_{253}$ mPDZ2 (left). Impairment of the binding to PSD-95 second PDZ domain by expressing PSD-95 mPDZ2 (H225V single point mutation on the full-length PSD-95) impacts both FRET with Stg::mCherry WT and S9D (middle) (Stg WT + PSD-95 WT = 2.054 ns, n = 230 spines, 23 cells; Stg WT + PSD-95 mPDZ2 = 2.172 ns, n = 286 spines, 30 cells; Stg S9D + PSD-95 WT = 1.987 ns, n = 268 spines, 28 cells; Stg S9D + PSD-95 mPDZ2 = 2.088 ns, n = 133 spines, 14 cells). The relative lifetime change shows that PDZ2 contributes equally to the binding of Stg WT and Stg S9D (right) (Stg WT = 0.115 a.u.; Stg S9D = 0.100 a.u.).

(D) Neurons transfected with the FRET pair Stg::mCherry WT or S9D and PSD-95::GFP$_{400}$ mPDZ3 with the GFP inserted after PDZ domain 3 (left). Impairment of the binding to PSD-95 third PDZ domain by expressing PSD-95 mPDZ3 (H372V single point mutation on the full-length PSD-95) impacts both FRET with Stg::mCherry WT and S9D (middle) (Stg WT + PSD-95 WT = 2.113 ns, n = 168 spines, 18 cells; Stg WT + PSD-95 mPDZ3 = 2.223 ns, n = 201 spines, 21 cells; Stg S9D + PSD-95 WT = 2.049 ns, n = 268 spines, 28 cells; Stg S9D + PSD-95 mPDZ3 = 2.204 ns, n = 127 spines, 14 cells). The relative lifetime change shows that PDZ3 contributes more to the binding of Stg S9D (right) (Stg WT = 0.093 a.u.; Stg S9D = 0.135 a.u.). Each graph corresponds to paired experiments.

Data are represented as mean ± SEM and compared using Student's t tests. **p < 0.01; ***p < 0.0005; ns, not significant.

movements were monitored by video microscopy (Bats et al., 2007) (Figure 6A). Movement of single AMPARs was slower in cells expressing stargazin 24G than in those expressing stargazin WT, as evidenced by the smaller surface explored by the receptor trajectories (Figures 6B and 6F). This effect was found in both the synaptic and extra-synaptic compartments, although it was more drastic in the latter (Figure S6). Accordingly, the distribution of AMPAR diffusion coefficients was displaced toward a higher fraction of immobile receptors in the presence of stargazin 24G than with WT (Figures 6C–6E). Altogether, these experiments indicate that stargazin 24G is sufficient to increase AMPAR diffusional trapping and immobile fraction.

In order to investigate whether the increase in AMPAR immobilization is translated into an accumulation of AMPARs at synapses, we used a super-resolution direct stochastic optical reconstruction microscopy (dSTORM) approach to count the number of putative AMPARs (Figure 7). As previously described (Nair et al., 2013), we used the median fluorescence intensity of isolated single emitting species in the shaft as a reference for the signal provided by an individually labeled AMPAR. Then, we estimated AMPAR content at synaptic nanodomains in dSTORM images under the same conditions used in the study of AMPAR mobility. As expected from an increase in the diffusional trapping of AMPARs, we found that stargazin 24G promoted a robust increase in the number of endogenous AMPARs per nanodomain as compared to stargazin WT (Figures 7A, 7B, and 7E). In addition, we found that stargazin 24G led to an increase in the size and number of AMPAR nanodomains (Figures 7C and 7D), although it had no impact on PSD-95 clusters (Figure S7).

Finally, to investigate whether the decrease in AMPAR lateral mobility induced by stargazin 24G has a functional impact at synapses, we measured miniature excitatory postsynaptic currents (mEPSCs) in neurons overexpressing stargazin 24G and PSD-95, as shown in Figures 6 and 7. Remarkably, we found that stargazin 24G produced a robust enhancement in both the amplitude and frequency of mEPSCs (Figures 8A–8C). This effect was due to binding to PSD-95, as mutation of the

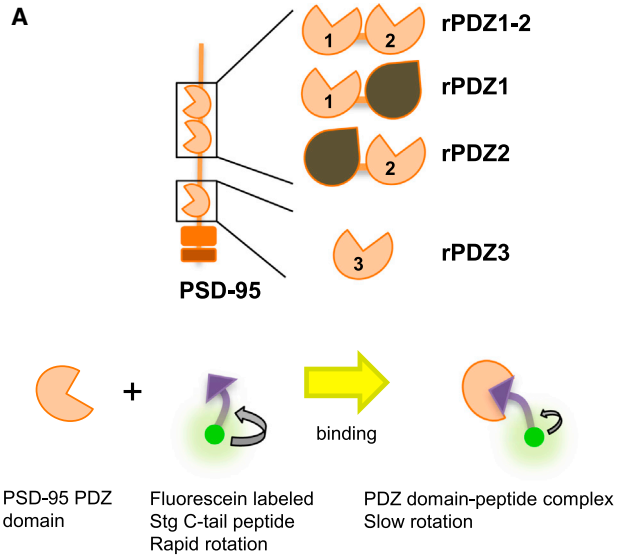

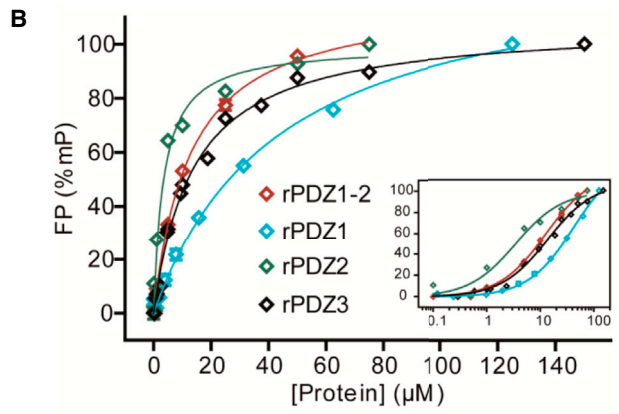

C

Domain(s) measured	Apparent Kd ± sem (μM)
rPDZ1-2	12.6 ± 0.7
rPDZ1	43.2 ± 3.0
rPDZ2	3.4 ± 0.5
rPDZ3	13.7 ± 0.6

Figure 5. Stargazin PDZ-Binding Motif Has a Greater Affinity for PDZ2 and PDZ3 Domains of PSD-95

(A) Schemes of the various recombinant PDZ domain constructs (rPDZ) used for the dissociation constant measurements (top). rPDZ1-2 corresponds to the tandem of the first two PDZ domains of PSD-95; rPDZ1 and rPDZ2 are derived from the previous constructs and contain each a single point mutation that impairs binding to PDZ domain 2 (H225V for rPDZ1) and PDZ domain 1 (H130V for rPDZ2); rPDZ3 corresponds to the third PDZ domain. Schemes of the fluorescent polarization assays are also shown (bottom).

(B) Fluorescence polarization (FP)-based titrations of the various PDZ domains of PSD-95 versus the last 15 amino acids of stargazin labeled with fluorescein. Each titration is plotted as the normalized average of at least three experiments with their SEM error bars and the corresponding fitted curve. The inset corresponds to the same datasets with a logarithmic representation of the protein concentration. mP, millipolarization value.

(C) Summary table of the dissociation constants obtained in (B).

PDZ-domain-binding motif completely reversed the potentiating effect of stargazin 24G. We verified that expression of PSD-95::GFP and Stg::mCherry WT did not modify mEPSC amplitude and frequency as previously published (Nair et al., 2013) (Figure S8A). Because stargazin can also modulate the gating and conductance of AMPARs, we verified that the potentiating effects of the 24G linker were not due to modifications of the AMPAR intrinsic properties. First, we found no differences in the time course of mEPSC traces in neurons expressing stargazin 24G or stargazin WT, suggesting that potentiation was not due to modulation of the deactivation/desensitization kinetics (Figure 8D). Second, we found no differences in the weighted mean single-channel conductance of synaptic AMPARs in neurons expressing stargazin 24G or WT, as estimated using a peak scaled non-stationary fluctuation analysis (Figures 8E and 8F). Taken together, these observations suggest that stargazin 24G potentiates synaptic currents exclusively by enhancing the diffusional trapping—and, hence, accumulation—of AMPARs at synapses. It is also conceivable that the accumulation of AMPARs by stargazin 24G and S9D could occur at silent synapses and result in the observed increase in mEPSC frequency. However, using dedicated analysis procedures, we found that a model of multiplicative scaling (which can reveal subthreshold mEPSCs) is sufficient to explain our findings for the extended C-tail constructs (Figure S8B) (Kim et al., 2012). This is corroborated by our dSTORM data, showing that the number of PSD-95 clusters (i.e., putative synapses) without GluA2 nanodomains is the same for neurons expressing stargazin WT or 24G (Figure S7C).

In summary, the present study demonstrates that enhancing the apparent length of the stargazin C-tail is sufficient to facilitate the interaction with a perpendicularly oriented PSD-95 by engaging the PDZ3 domain, thus promoting the recruitment of additional AMPARs to, ultimately, potentiate synaptic transmission.

DISCUSSION

PSD-95 is the most prominent scaffolding protein at the PSD and a potent regulator of synaptic transmission (Ehrlich and Malinow, 2004; Kim and Sheng, 2004; Stein et al., 2003). Thus, it is crucial to understand how PSD-95 overall conformation relates to synaptic function. Recent studies suggesting that PSD-95 is anchored in the plasma membrane and oriented perpendicularly to it at the PSD have raised questions as to how this particular spatial conformation might impact binding to its different partners and, more important, what the consequences are for synaptic function (Chen et al., 2008). We found that PSD-95 orientation might impose important constraints to the binding of transmembrane proteins. This is particularly important for proteins such as stargazin, which has a C-tail partially bound to the plasma membrane via electrostatic interactions (Sumioka et al., 2010). Stargazin with a longer effective C-tail can better access and bind the farthest located and highest affinity PDZ2/3 domains; as a consequence, it facilitates both AMPAR anchoring and synaptic transmission.

We reasoned that, if the effective length of the stargazin C-tail is critical for binding PSD-95, it is most likely subject to

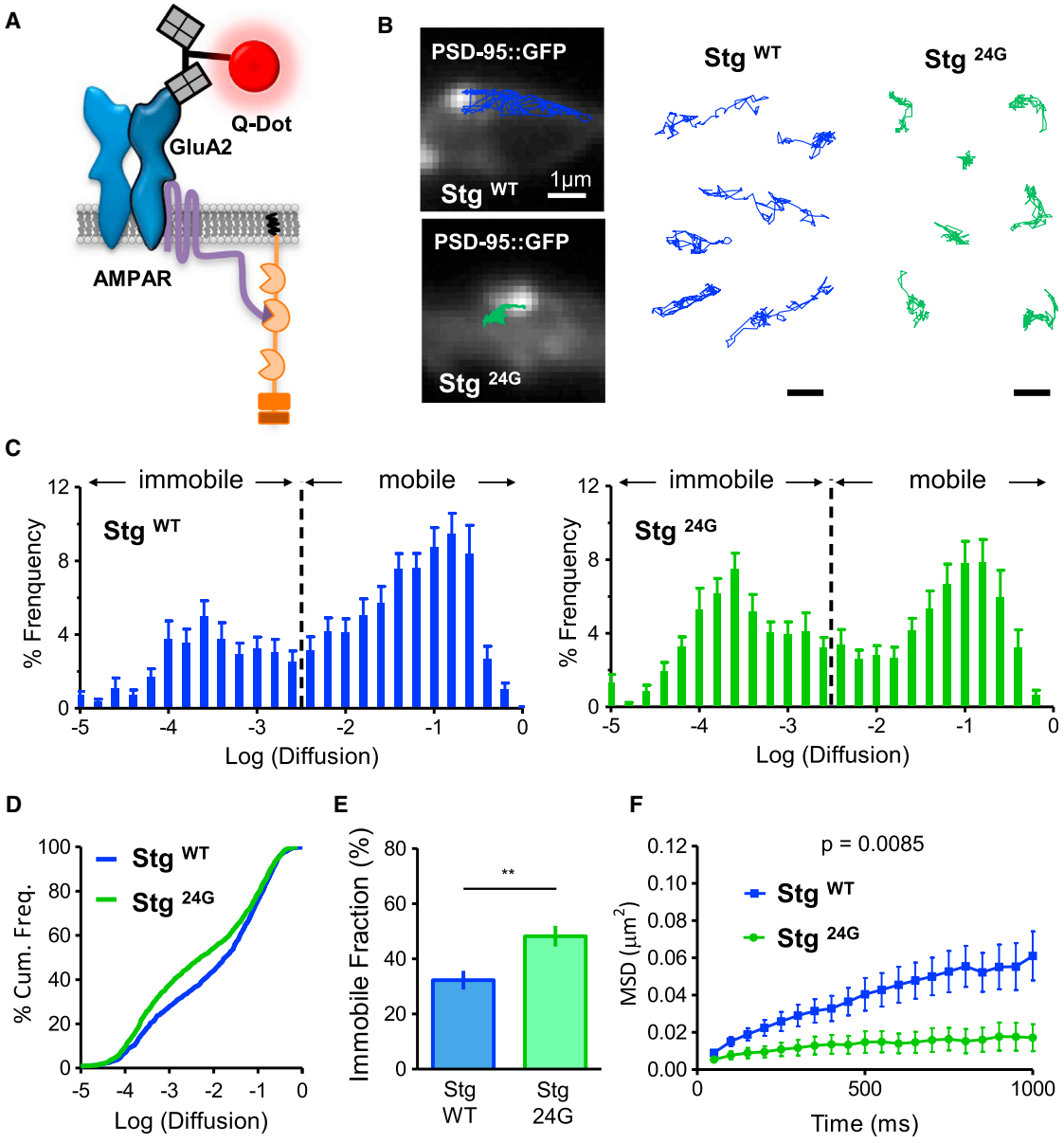

Figure 6. The Artificial Extension of the Stargazin C-tail Is Sufficient for the Surface Immobilization of AMPARs

(A) Scheme representing the labeling strategy and targeted site on endogenous GluA2-containing receptors. Endogenous GluA2 subunits were tracked using primary antibody against GluA2 N-terminal domain and QDot-coupled secondary antibody.

(B) Overlay trajectories (blue for WT, n = 16 cells; and green for 24G, n = 18 cells) of GluA2 QD tracking for 30 s and the synaptic marker PSD-95::GFP (left) and a few representative trajectories of GluA2 QD tracking membrane diffusion in neurons expressing Stg::mCherry WT or 24G and PSD-95::GFP_{400}. The surface explored by GluA2 is decreased when expressing Stg::mCherry 24G. Scale bar, 1 µm.

(C) Frequency distributions of the diffusion coefficients calculated from the trajectories of GluA2-containing receptors. Neurons expressing Stg::mCherry 24G have an increased immobile population (diffusion coefficient, D, $< 1 \times 10^{-2}$ $\mu m^2/s$).

(D) Cumulative distribution of the diffusion coefficient of GluA2-containing receptors shown in (C). Cum. Freq., cumulative frequency.

(E) The mean immobile fraction ± SEM is increased in neurons expressing Stg::mCherry 24G (WT = 32.3; 24G = 48.2). Data were compared using Student's t test.

(F) Mean square displacement (MSD) of GluA2-containing receptors versus time plot for neurons expressing Stg::mCherry WT and 24G. The area explored by GluA2-containing receptors is reduced in neurons expressing Stg::mCherry 24G. The two conditions were compared by calculating the area under the curve for each cell in both conditions. Areas under the curves were compared using Student's t tests.

Data are represented as mean ± SEM. **$p < 0.01$.

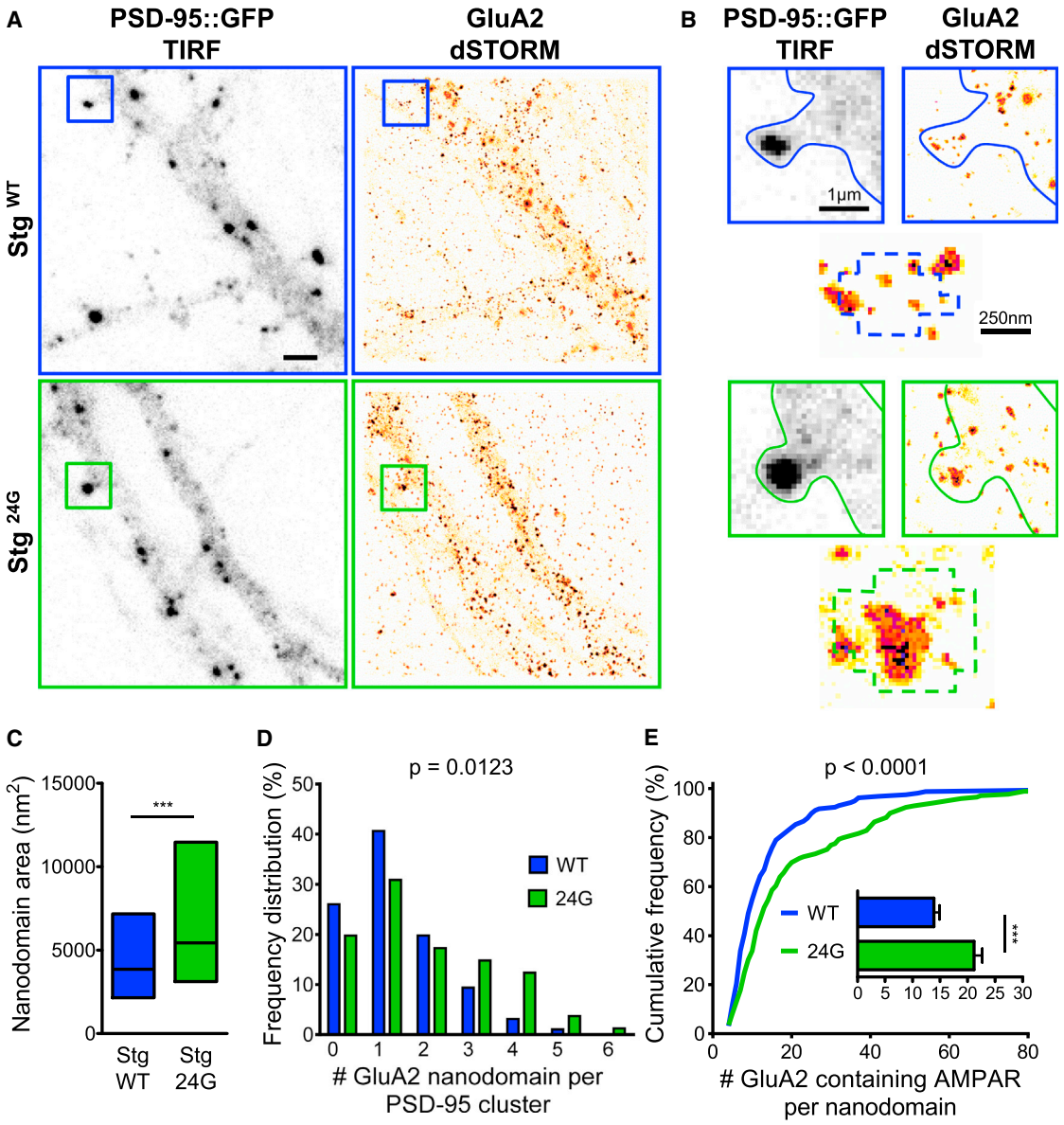

Figure 7. The Artificial Extension of the Stargazin C-tail Increases AMPAR Nanodomain Number and Size

(A) Images of cultured hippocampal neurons (12 DIV) expressing PSD-95::GFP$_{400}$ (left) and Stg::mCherry WT or 24G and live labeled for surface endogenous GluA2 reconstructed from dSTORM imaging (right), revealing AMPAR nanodomain organization. Scale bar, 2 µm.

(B) Zooms on portion of dendrites (top) and on PSD-95 clusters (bottom).

(C) Nanodomain area calculated after extraction of major-axis and minor-axis length for each nanodomain, considering a nanodomain as an elliptic domain (WT = 3,853 nm^2, n = 122 nanodomains, 12 cells; 24G = 5,432 nm^2, n = 151 nanodomains, 12 cells). Bar graph shows medians (±20%–75% inter-quartile range [IQR]).

(D) Frequency distributions of the number of GluA2 nanodomains per PSD-95 cluster.

(E) Cumulative distributions of the estimated number of GluA2-containing receptor per nanodomains (WT = 14 receptors, n = 157 nanodomains, 12 cells; 24G = 21 receptors, n = 169 nanodomains, 12 cells). Inset shows mean ± SEM.

Data were compared using Mann-Whitney tests. ***p < 0.0005. In (E), p < 0.0001 is the comparison for cumulative distribution curves.

See also Figure S6.

modulation. We found that changes in charge of the serine-rich region of the stargazin C-tail, such as those induced by phosphorylation, strongly modulate its effective length and extension into the cytoplasm, away from the plasma membrane. Previous studies have shown that the stargazin C-tail is attached to the membrane via electrostatic interactions between positively charged arginine residues and the negatively charged phospholipids (Sumioka et al., 2010). Phosphorylation of neighboring serine residues are thought to neutralize the positively charged arginines and detach the stargazin C-tail from the plasma

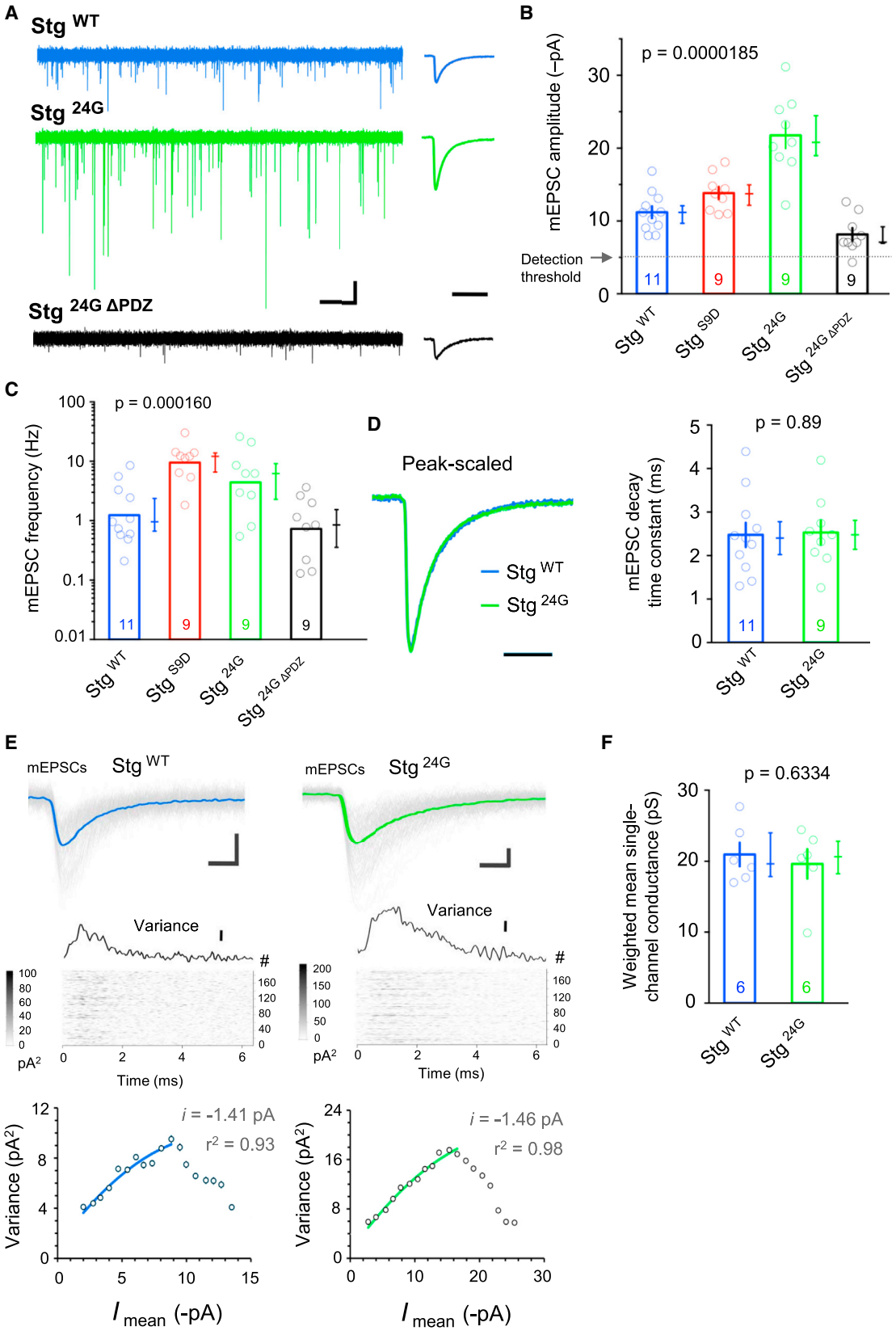

(legend on next page)

membrane. Here, we found that stargazin phosphorylation not only detaches the C-tail from the membrane but also effectively extends the C-tail into the cytoplasm to facilitate access and binding to PSD-95. It is important to stress that membrane detachment should not necessarily lead to an extension of the C-tail into the cytoplasm, especially in the crowded PSD environment. In fact, we showed that the stargazin C-tail effectively extended into the cytoplasm in a charge-dependent manner and that this extension enables the distal half of the stargazin C-tail carrying the PDZ-domain-binding motif to sample more efficiently the cytoplasm to reach its binding partners. In line with these results, we found that a small truncation in the distal half of the stargazin C-tail is sufficient to reverse the effects of phosphorylation, suggesting that stargazin phosphorylation facilitates binding to PSD-95 simply by elongating the C-tail. Although we cannot rule out that stargazin phosphorylation might recruit additional proteins that might help stabilize the stargazin-PSD-95 complex, we find it difficult to be the main force that modulates binding. First, we found that the charge of the C-tail is the main factor regulating binding to PSD-95 regardless of the residue being modified. We found that disrupting the positive charge of the C-tail by mutating the arginine residues was sufficient to facilitate binding to PSD-95, a contradictory finding if phosphorylated serine residues were needed to recruit additional stabilizers. Second, we found that the facilitated binding of stargazin S9D can be reversed simply by truncating, and thus shortening, a small region of the C-tail. Potential stabilizers should still be recruited to the phospho-mimetic residues.

Mechanistically, we found that stargazin with an effectively elongated C-tail facilitates overall binding to PSD-95 by engaging the farthest located and highest affinity PDZ2/3 domains. By reaching the deepest PDZ domains, stargazin with an elongated C-tail might also encounter less competition from other transmembrane proteins known to bind PSD-95 for the limited number of PSD-95 slots at synapses.

What is the physiological consequence of modulating the apparent length of the stargazin C-tail by phosphorylation? Since stargazin can be phosphorylated by CaMKII and PKC (Tomita et al., 2005b), it is likely that the effective length of the stargazin C-tail might be at the core of LTP of synaptic transmission (Malinow et al., 2000; Opazo and Choquet, 2011). In fact, it has been previously demonstrated that stargazin phosphorylation is critical for LTP (Tomita et al., 2005b). Mechanistically, we have previously shown that stargazin phosphorylation triggers the diffusional trapping—and, therefore, accumulation—of membrane-diffusing AMPARs (Opazo et al., 2010). Our present study strongly suggests that CaMKII/PKC could support LTP simply by effectively elongating the stargazin C-tail and thus promoting recruitment of additional synaptic AMPARs. This hypothesis is supported by the present finding that stargazin C-tail interaction with the membrane is reduced upon cLTP in a CaMKII-dependent manner and that artificially elongating the stargazin C-tail by means of a linker is sufficient to both recruit additional synaptic AMPARs and facilitate synaptic transmission.

Taken together, our studies reveal an additional level of complexity in the regulation of binding between stargazin and PSD-95, the most prominent scaffold protein at the PSD. We show that binding between stargazin and PSD-95 is controlled not only by the presence but also by the particular orientation of these interactors at the PSD. Although we demonstrated that this is true for stargazin, it is likely that the same rules apply to other transmembrane proteins known to bind PSD-95, such as NMDARs, Neuroligin1, potassium channels such as Kv1 and Kir, and a number of neuromodulator receptors. It will be interesting to examine how the effective length of the intracellular domains of these transmembrane proteins might impact the competition for the limited number of PSD-95 slots. On the other hand, although we have examined the conformational changes of the stargazin C-tail controlling binding to PSD-95, it is possible that this interaction is also regulated by post-translational modifications impacting the orientation of PSD-95 toward the plasma membrane. In fact, we found that preventing the N-terminal palmitoylation of PSD-95, presumably disrupting its perpendicular orientation to the membrane, was sufficient to abolish the enhanced ability of stargazin carrying an elongated C-tail, such as S9D or 24G, to bind PSD-95.

In conclusion, we have shown that the effective, rather than actual, length of the stargazin C-tail is crucial for binding a perpendicular-oriented PSD-95 scaffold and that, as such, it potently governs both AMPAR anchoring and synaptic transmission.

Figure 8. The Artificial Extension of the Stargazin C-tail Is Sufficient for Potentiation of Synaptic Transmission

(A) Recordings of mEPSCs in cultured hippocampal neurons coexpressing Stg::mCherry mutants with PSD-95::GFP. Left: example 20-s recording traces of mEPSCs in cells expressing stg WT and 24G either with or without PDZ ligand. Horizontal scale bar, 2 s; vertical scale bar, 10 pA. Right: time-expanded view of mean mEPSCs. Horizontal scale bar, 10 ms.

(B) The stg 24G potentiates mEPSC amplitude by ~2-fold through a mechanism requiring its PDZ ligand, Welch's ANOVA. The dashed line represents the amplitude threshold for the detection of mEPSCs.

(C) Frequency of mEPSCs as in (B). Welch's ANOVA obtained for the log-transformed data.

(D) Left: peak-scaled mean mEPSCs. Time base is 5 ms. Right: Welch's two-tailed t test.

(E) Estimation of weighted mean single-channel current of synaptic AMPARs by peak-scaled non-stationary fluctuation analysis (NSFA) of mEPSCs. Top row: Aligned mEPSCs (gray) for cells expressing the stg WT (left) and 24G (right) are aligned with their mean mEPSCs in blue and green, respectively. Horizontal scale bars, 1 ms; vertical scale bars, 10 pA. Middle: inverted gray color maps for the squared differences between the decay of each mEPSC and the peak-scaled mean mEPSC. The ensemble variance is illustrated above each color map. Scale bars, 2 pA^2. Bottom: plots of the mean current against the ensemble variance for the binned data points.

(F) Weighted mean conductance of individual AMPARs, Welch's two-tailed t test.

Unless specified otherwise, all graphs represent mean ± SEM, with the number of cells at the base. Next to each bar, the median is plotted with 83% bootstrap confidence intervals.

See also Figure S8.

EXPERIMENTAL PROCEDURES

Molecular Biology, Biochemistry, Cell Culture, and Transfection

Cloning of plasmids and cultures of rat hippocampal neurons was performed as in Opazo et al. (2010) (see Supplemental Experimental Procedures for details).

FRET Measurements

FRET measurements were performed either in the time domain, as in Sainlos et al. (2011), or in the frequency domain (see Supplemental Experimental Procedures for details).

dSTORM, Single-Particle Tracking, and Analysis

dSTORM was performed as in Nair et al. (2013). Single-particle tracking was performed as in Opazo et al. (2010) (see Supplemental Experimental Procedures for details).

Electrophysiological Recordings

Electrophysiological recordings were performed as in Constals et al. (2015) (see Supplemental Experimental Procedures for details).

Statistics

Statistical values are given as mean ± SEM unless stated otherwise (see Supplemental Experimental Procedures for details).

Ethical Approval

All experiments were approved by the Regional Ethical Committee on Animal Experiments of Bordeaux.

SUPPLEMENTAL INFORMATION

Supplemental Information includes Supplemental Experimental Procedures and eight figures and can be found with this article online at http://dx.doi.org/10.1016/j.neuron.2015.03.013.

AUTHOR CONTRIBUTIONS

A.S.H., P.O., and D.C. conceived the study, formulated the models, and wrote the manuscript. A.S.H. performed most FRET measurements, single-molecule experiments, and dSTORM experiments; analyzed the data; and prepared the corresponding figures. A.C.P. performed all electrophysiology experiments and corresponding data analysis and created the figures. D.G.B. synthesized the peptides for fluorescence polarization-based titrations. D.G.B. and M.S. designed and performed fluorescence polarization-based titrations and corresponding data analysis and created the figures. N.R. performed most molecular biology constructs. C.P. performed part of the FRET experiments (Figure 3E) and helped run the FRET-FLIM setup. A.P. and F.C. performed all pull-down experiments and corresponding data analysis and created the figures. All authors contributed to the preparation of the manuscript.

ACKNOWLEDGMENTS

We acknowledge I. Gauthereau for recombinant protein production; E. Gouaux for the anti-GluA2 antibody; J.-B. Sibarita for providing Palm-Tracer analysis software for dSTORM analysis; the Bordeaux Imaging Center, part of the France-BioImaging national infrastructure supported by the French National Research Agency (ANR-10-INSB-04, ''Investments for the Future''), for support in microscopy; The Biochemistry Platform of Bordeaux Neurocampus for access to the plate reader and gel readers; The ''Plateforme Proteome'' for access to MALDI-TOF; B. Tessier, D. Bouchet, A. Frouin, C. Breillat, E. Verdier, and C. Genuer for cell culture and plasmid production; and R. Sterling for technical assistance. This work was supported by funding from the Ministère de l'Enseignement Supérieur et de la Recherche (ANR NanoDom, ChemTraffic and Stim-Traf-Park, Labex BRAIN and ANR-10-INBS-04 France-BioImaging), Centre National de la Recherche Scientifique, the Conseil Régional d'Aquitaine, European Research Council (ERC) grant nano-dyn-syn to D.C., a Marie-Curie Intra-European fellowship to D.G.B. (neuroCHEMbiotools, #273817), and an EMBO fellowship ALTF 129-2009 and a Marie Curie grant Synapsemap to A.C.P.

Received: April 7, 2014
Revised: November 17, 2014
Accepted: February 23, 2015
Published: April 2, 2015

REFERENCES

Bats, C., Groc, L., and Choquet, D. (2007). The interaction between Stargazin and PSD-95 regulates AMPA receptor surface trafficking. Neuron *53*, 719–734.

Chen, L., Chetkovich, D.M., Petralia, R.S., Sweeney, N.T., Kawasaki, Y., Wenthold, R.J., Bredt, D.S., and Nicoll, R.A. (2000). Stargazin regulates synaptic targeting of AMPA receptors by two distinct mechanisms. Nature *408*, 936–943.

Chen, X., Winters, C., Azzam, R., Li, X., Galbraith, J.A., Leapman, R.D., and Reese, T.S. (2008). Organization of the core structure of the postsynaptic density. Proc. Natl. Acad. Sci. USA *105*, 4453–4458.

Chen, X., Nelson, C.D., Li, X., Winters, C.A., Azzam, R., Sousa, A.A., Leapman, R.D., Gainer, H., Sheng, M., and Reese, T.S. (2011). PSD-95 is required to sustain the molecular organization of the postsynaptic density. J. Neurosci. *31*, 6329–6338.

Cheng, D., Hoogenraad, C.C., Rush, J., Ramm, E., Schlager, M.A., Duong, D.M., Xu, P., Wijayawardana, S.R., Hanfelt, J., Nakagawa, T., et al. (2006). Relative and absolute quantification of postsynaptic density proteome isolated from rat forebrain and cerebellum. Mol. Cell. Proteomics *5*, 1158–1170.

Constals, A., Penn, A.C., Compans, B., Toulmé, E., Phillipat, A., Marais, S., Retailleau, N., Hafner, A.S., Coussen, F., Hosy, E., and Choquet, D. (2015). Glutamate-induced AMPA receptor desensitization increases their mobility and modulates short-term plasticity through unbinding from stargazin. Neuron *85*, 787–803.

Craven, S.E., El-Husseini, A.E., and Bredt, D.S. (1999). Synaptic targeting of the postsynaptic density protein PSD-95 mediated by lipid and protein motifs. Neuron *22*, 497–509.

Ehrlich, I., and Malinow, R. (2004). Postsynaptic density 95 controls AMPA receptor incorporation during long-term potentiation and experience-driven synaptic plasticity. J. Neurosci. *24*, 916–927.

El-Husseini, A.E., Craven, S.E., Chetkovich, D.M., Firestein, B.L., Schnell, E., Aoki, C., and Bredt, D.S. (2000). Dual palmitoylation of PSD-95 mediates its vesiculotubular sorting, postsynaptic targeting, and ion channel clustering. J. Cell Biol. *148*, 159–172.

Elias, G.M., and Nicoll, R.A. (2007). Synaptic trafficking of glutamate receptors by MAGUK scaffolding proteins. Trends Cell Biol. *17*, 343–352.

Feng, W., and Zhang, M. (2009). Organization and dynamics of PDZ-domain-related supramodules in the postsynaptic density. Nat. Rev. Neurosci. *10*, 87–99.

Fomina, S., Howard, T.D., Sleator, O.K., Golovanova, M., O'Ryan, L., Leyland, M.L., Grossmann, J.G., Collins, R.F., and Prince, S.M. (2011). Self-directed assembly and clustering of the cytoplasmic domains of inwardly rectifying Kir2.1 potassium channels on association with PSD-95. Biochim. Biophys. Acta *1808*, 2374–2389.

Kim, E., and Sheng, M. (2004). PDZ domain proteins of synapses. Nat. Rev. Neurosci. *5*, 771–781.

Kim, J., Tsien, R.W., and Alger, B.E. (2012). An improved test for detecting multiplicative homeostatic synaptic scaling. PLoS ONE *7*, e37364.

Korkin, D., Davis, F.P., Alber, F., Luong, T., Shen, M.Y., Lucic, V., Kennedy, M.B., and Sali, A. (2006). Structural modeling of protein interactions by analogy: application to PSD-95. PLoS Comput. Biol. *2*, e153.

Long, J.F., Tochio, H., Wang, P., Fan, J.S., Sala, C., Niethammer, M., Sheng, M., and Zhang, M. (2003). Supramodular structure and synergistic target binding of the N-terminal tandem PDZ domains of PSD-95. J. Mol. Biol. *327*, 203–214.

Malinow, R., Mainen, Z.F., and Hayashi, Y. (2000). LTP mechanisms: from silence to four-lane traffic. Curr. Opin. Neurobiol. *10*, 352–357.

McCann, J.J., Zheng, L., Chiantia, S., and Bowen, M.E. (2011). Domain orientation in the N-terminal PDZ tandem from PSD-95 is maintained in the full-length protein. Structure *19*, 810–820.

Nair, D., Hosy, E., Petersen, J.D., Constals, A., Giannone, G., Choquet, D., and Sibarita, J.B. (2013). Super-resolution imaging reveals that AMPA receptors inside synapses are dynamically organized in nanodomains regulated by PSD95. J. Neurosci. *33*, 13204–13224.

Nakagawa, T., Futai, K., Lashuel, H.A., Lo, I., Okamoto, K., Walz, T., Hayashi, Y., and Sheng, M. (2004). Quaternary structure, protein dynamics, and synaptic function of SAP97 controlled by L27 domain interactions. Neuron *44*, 453–467.

Opazo, P., and Choquet, D. (2011). A three-step model for the synaptic recruitment of AMPA receptors. Mol. Cell. Neurosci. *46*, 1–8.

Opazo, P., Labrecque, S., Tigaret, C.M., Frouin, A., Wiseman, P.W., De Koninck, P., and Choquet, D. (2010). CaMKII triggers the diffusional trapping of surface AMPARs through phosphorylation of stargazin. Neuron *67*, 239–252.

Opazo, P., Sainlos, M., and Choquet, D. (2012). Regulation of AMPA receptor surface diffusion by PSD-95 slots. Curr. Opin. Neurobiol. *22*, 453–460.

Pegan, S., Tan, J., Huang, A., Slesinger, P.A., Riek, R., and Choe, S. (2007). NMR studies of interactions between C-terminal tail of Kir2.1 channel and PDZ1,2 domains of PSD95. Biochemistry *46*, 5315–5322.

Roberts, M.F., Taylor, D.W., and Unger, V.M. (2011). Two modes of interaction between the membrane-embedded TARP stargazin's C-terminal domain and the bilayer visualized by electron crystallography. J. Struct. Biol. *174*, 542–551.

Sainlos, M., Tigaret, C., Poujol, C., Olivier, N.B., Bard, L., Breillat, C., Thiolon, K., Choquet, D., and Imperiali, B. (2011). Biomimetic divalent ligands for the acute disruption of synaptic AMPAR stabilization. Nat. Chem. Biol. *7*, 81–91.

Schnell, E., Sizemore, M., Karimzadegan, S., Chen, L., Bredt, D.S., and Nicoll, R.A. (2002). Direct interactions between PSD-95 and stargazin control synaptic AMPA receptor number. Proc. Natl. Acad. Sci. USA *99*, 13902–13907.

Sheng, M., and Sala, C. (2001). PDZ domains and the organization of supramolecular complexes. Annu. Rev. Neurosci. *24*, 1–29.

Songyang, Z., Fanning, A.S., Fu, C., Xu, J., Marfatia, S.M., Chishti, A.H., Crompton, A., Chan, A.C., Anderson, J.M., and Cantley, L.C. (1997). Recognition of unique carboxyl-terminal motifs by distinct PDZ domains. Science *275*, 73–77.

Stein, V., House, D.R., Bredt, D.S., and Nicoll, R.A. (2003). Postsynaptic density-95 mimics and occludes hippocampal long-term potentiation and enhances long-term depression. J. Neurosci. *23*, 5503–5506.

Sumioka, A., Yan, D., and Tomita, S. (2010). TARP phosphorylation regulates synaptic AMPA receptors through lipid bilayers. Neuron *66*, 755–767.

Tomita, S., Adesnik, H., Sekiguchi, M., Zhang, W., Wada, K., Howe, J.R., Nicoll, R.A., and Bredt, D.S. (2005a). Stargazin modulates AMPA receptor gating and trafficking by distinct domains. Nature *435*, 1052–1058.

Tomita, S., Stein, V., Stocker, T.J., Nicoll, R.A., and Bredt, D.S. (2005b). Bidirectional synaptic plasticity regulated by phosphorylation of stargazin-like TARPs. Neuron *45*, 269–277.

Wang, W., Weng, J., Zhang, X., Liu, M., and Zhang, M. (2009). Creating conformational entropy by increasing interdomain mobility in ligand binding regulation: a revisit to N-terminal tandem PDZ domains of PSD-95. J. Am. Chem. Soc. *131*, 787–796.

Xu, W., Schlüter, O.M., Steiner, P., Czervionke, B.L., Sabatini, B., and Malenka, R.C. (2008). Molecular dissociation of the role of PSD-95 in regulating synaptic strength and LTD. Neuron *57*, 248–262.

Yasuda, R. (2006). Imaging spatiotemporal dynamics of neuronal signaling using fluorescence resonance energy transfer and fluorescence lifetime imaging microscopy. Curr. Opin. Neurobiol. *16*, 551–561.